An optimal artificial neural network controller for load frequency control of a four-area interconnected power system

Basavarajappa Sokke Rameshappa, Nagaraj Mudakapla Shadaksharappa
Department of Electrical and Electronics Engineering, Bapuji Institute of Engineering and Technology,
Davanagere Visvesvaraya Technological University, Belagavi, India

Article Info	ABSTRACT
Article history: Received Sep 2, 2021 Revised Mar 11, 2022 Accepted Apr 10, 2022 *Keywords:* Interconnected power system Load frequency control NARMA-L2 controller Optimal ANN controller PID controller	In this paper, an optimal artificial neural network (ANN) controller for load frequency control (LFC) of a four-area interconnected power system with non-linearity is presented. A feed forward neural network with multi-layers and Bayesian regularization backpropagation (BRB) training function is used. This controller is designed on the basis of optimal control theory to overcome the problem of load frequency control as load changes in the power system. The system comprised of transfer function models of two thermal units, one nuclear unit and one hydro unit. The controller model is developed by considering generation rate constraint (GRC) of different units as a non-linearity. The typical system parameters obtained from IEEE press power engineering series and EPRI books. The robustness, effectiveness, and performance of the proposed optimal ANN controller for a step load change and random load change in the system is simulated through using MATLAB-Simulink. The time response characteristics are compared with that obtained from the proportional, integral and derivative (PID) controller and non-linear autoregressive-moving average (NARMA-L2) controller. The results show that the algorithm developed for proposed controller has a superiority in accuracy as compared to other two controllers. *This is an open access article under the <u>CC BY-SA</u> license.*

Corresponding Author:

Basavarajappa Sokke Rameshappa
Department of Electrical and Electronics Engineering, Bapuji Institute of Engineering and Technology
Shamanur Road, Davanagere-577004, Karnataka, India
Email: basavarajsr@gmail.com

1. INTRODUCTION

Automatic load frequency control is the main area of concern in the operation of an interconnected power system. As load on the system changes, the frequency changes. In order to balance the megawatt (MW) generation with load demand, it is necessary to control the synchronous generators power output and frequency. This control is automatic, as it maintains the frequency at base value and power flows via tie-lines within scheduled values for a perturbation in the load [1]–[3]. The load frequency control monitors the area control error (ACE), which is the net real power interchange between the control areas plus the frequency deviation multiplied with a frequency bias. To reduce ACE, closer to zero, change the position of speed changer of the generator governors within the control area by means of load frequency control (LFC).

In the design of load frequency controllers, conventional control techniques have been developed, which gives slower responses. The developments in advanced technology, artificial intelligent (AI) based techniques such as neural networks, fuzzy logic, genetic algorithm (GA) and particle swarm optimization (PSO) have been using and these techniques overcome the disadvantages of conventional controllers and increase the speed of response. When the load changes suddenly, the primary automatic load frequency control can be obtained by the action of speed governor in the prime movers. A supplementary or secondary

automatic load frequency control action is used in the proposed system to bring the change in frequency and change in tie-line power to zero with the help of advanced controllers. The past studies in the literature explain the LFC problem with proportional-integral-derivative (PID) and fuzzy logic controllers, but less with optimal artificial neural network (ANN) controller and nonlinearity.

Prasad and Ansari [4], employed a three-layer ANN observer-based control strategy used in a two similar area interconnected power system with generation rate constraint (GRC) and governor dead band (GDB). This system is simulated for random unmatched disturbance estimation and its rejection. Qian and Fan [5], implemented a three-layer radial basis function (RBF) neural network for load frequency control of a two-area power system with GRC and wind turbine model. The control scheme is designed on the basis of terminal sliding mode control. Bhatia *et al.* [6] proposed a three-layer neural network-based NARMA-L2 controller for a three similar area power system with GRC. Only frequency deviation is discussed. Chettibi *et al.* [7] proposed and implemented a technique for forecast of grid voltage frequency in short time based on ANN models and deep recurrent neural networks. This can be used in an advanced control scheme and monitoring distributed generators for frequency and voltage variations. The performance of these networks was assessed in terms of root mean square error (RMSE) that was lies between 0.002 Hz and 0.01 Hz for sapling interval of 0.1 s and 1 s respectively.

Alzaareer *et al.* [8] proposed an ANN based NARMA-L2 controller model for a three-area interconnected system without GRC. This controller is compared with PI and PID controller for load frequency control in the system. Prakash and Sinha [9], proposed a hybrid neuro fuzzy (HNF) controller in a four–area power system without GRC. This controller performance is compared with fuzzy logic, three-layer ANN and PID controllers for 1% change in load. Peak overshoot and settling time values of -0.055 pu (-2.75 Hz) and 40 s respectively, obtained with ANN controller. Kumari *et al.* [10], proposed an ANN-PID control technique for a two area non-reheat thermal plant power system without GRC. The controller performance is tested with 10% step load perturbation and different error values are measured. Prakash and Sinha [11], proposed an ANN and adaptive neuro fuzzy inference system (ANFIS) for a six-area power system composed of hydro, thermal, gas, diesel, and nuclear plants without GRC. The controller performance is tested with 1% step load perturbation. Mucka *et al.* [12], employed a three-layer neural network-based NARMA-L2 controller for a four-area power system without GRC. The system is simulated with 2% change in load at frequency 50 Hz and its response has more settling time and undershoot.

The above research work [4]–[7], employs ANN based controller for two-area and three-area interconnected power system with GRC. Only two input variables and first order governor-turbine transfer function models are considered and the work [8]–[12], even though propose ANN based controllers with Levenberg-Marquardt learning function but does not provide information on the number of neurons in the hidden layer(s) and considered only first order non-reheat turbines without GRC. Hence, the present work proposes an optimal ANN controller with BRB training function and is designed based on state space model for load frequency control in a four-area power system comprises reheat tandem compound turbines with GRC and IEEE standard parameters are chosen within the operating constraints of system components.

2.   MODELLING OF THE SYSTEM

The main components of each area are governor, turbine, generator, and load. The dynamic models of governors, tandem compound steam turbines and hydro turbines were presented in [13], [14]. For thermal, nuclear, and hydro power plants, the transfer function models of a governor or hydraulic valve actuator are obtained from the basic Watt's governor operation. The thermal plant governor and turbine block diagram with fraction of power generated by high pressure (HP), intermediate pressure (IP), and low pressure (LP) sections is shown in Figure 1. Figure 2 shows the block diagram of nuclear plant governor and turbine with fraction of power generated by very high pressure (VHP), high pressure (HP), and low pressure (LP) sections. Figure 3 shows the block diagram of hydro plant governor and turbine.

The generation rate constraint is the limitation on the rate of change in the real power generation due to physical limitations of turbine. The existence of GRC [5], [7], [15] has an adverse effect on system stability. It should be considered for LFC problem as a non-linear model shown in Figure 4. The GRC values are taken into account by adding limiters to the turbines. The GRC values for thermal and nuclear plants are $\pm 0.005\ pu.MW.s^{-1}$ and that for hydro plant is $+0.045\ pu.MW.s^{-1}$ and $-0.06\ pu.MW.s^{-1}$. The transfer function model of synchronous generator and load is obtained by rotor dynamics, swing equation and overall frequency dependent characteristic of a composite load. Synchronous generator-load transfer function model [1], [2] in standard first order form is obtained as (1).

$$G_{SL}(s) = \frac{1}{2\,s\,H_i + D_i} = \frac{K_{ps,1}}{1 + s\,T_{ps,1}}\ \ for\ i = 1,2,3,4 \tag{1}$$
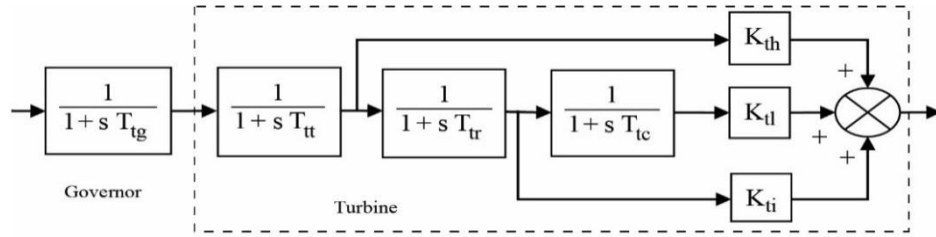
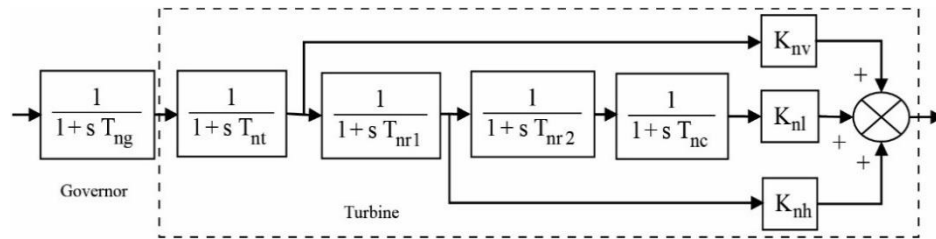Figure 1. Thermal plant governor and turbine model

Figure 2. Nuclear plant governor and turbine model
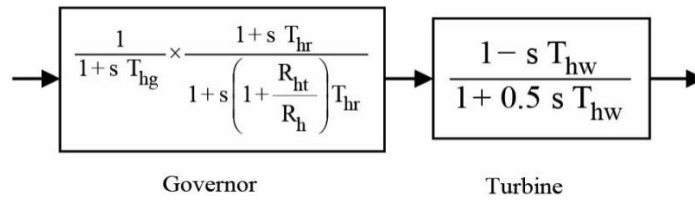

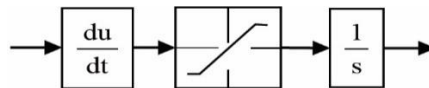Figure 3. Hydro plant governor and turbine model

Figure 4. Generation rate constraint model

The output of generator-load model is the change in frequency or the frequency deviation $\Delta f_i(s)$ due to change in load $\Delta P_{Li}(s)$. In normal operation, the change in tie-line power is obtained from synchronizing torque coefficient (T) using (2). ACE [9] is the input signal to controller for each power system area and is calculated using (3).

$$\Delta P_{ij}(s) = \frac{2\pi T}{s}\left(\Delta f_i(s) - \Delta f_j(s)\right) \; for \; i = 1,2,3,4 \tag{2}$$

$$ACE_i = \Delta P_{ij} + B_i \Delta f_i \tag{3}$$

The objective function (OF) determines the system dynamics and satisfy criterion such as fast response with minimized undershoot and steady state error. Thus, integral of time weighted absolute error (ITAE) is used as OF [15] and is calculated as (4).

$$ITAE_i = \int_0^{t_{max}} t\left|\Delta P_{ij} + B_i \Delta f_i\right| dt \tag{4}$$

By connecting the block diagrams of governor, turbine, generation rate constraint, generator and load models of respective areas and interconnecting these areas via tie-line model gives the complete block diagram of a four-area interconnected power system as shown in Figure 5.
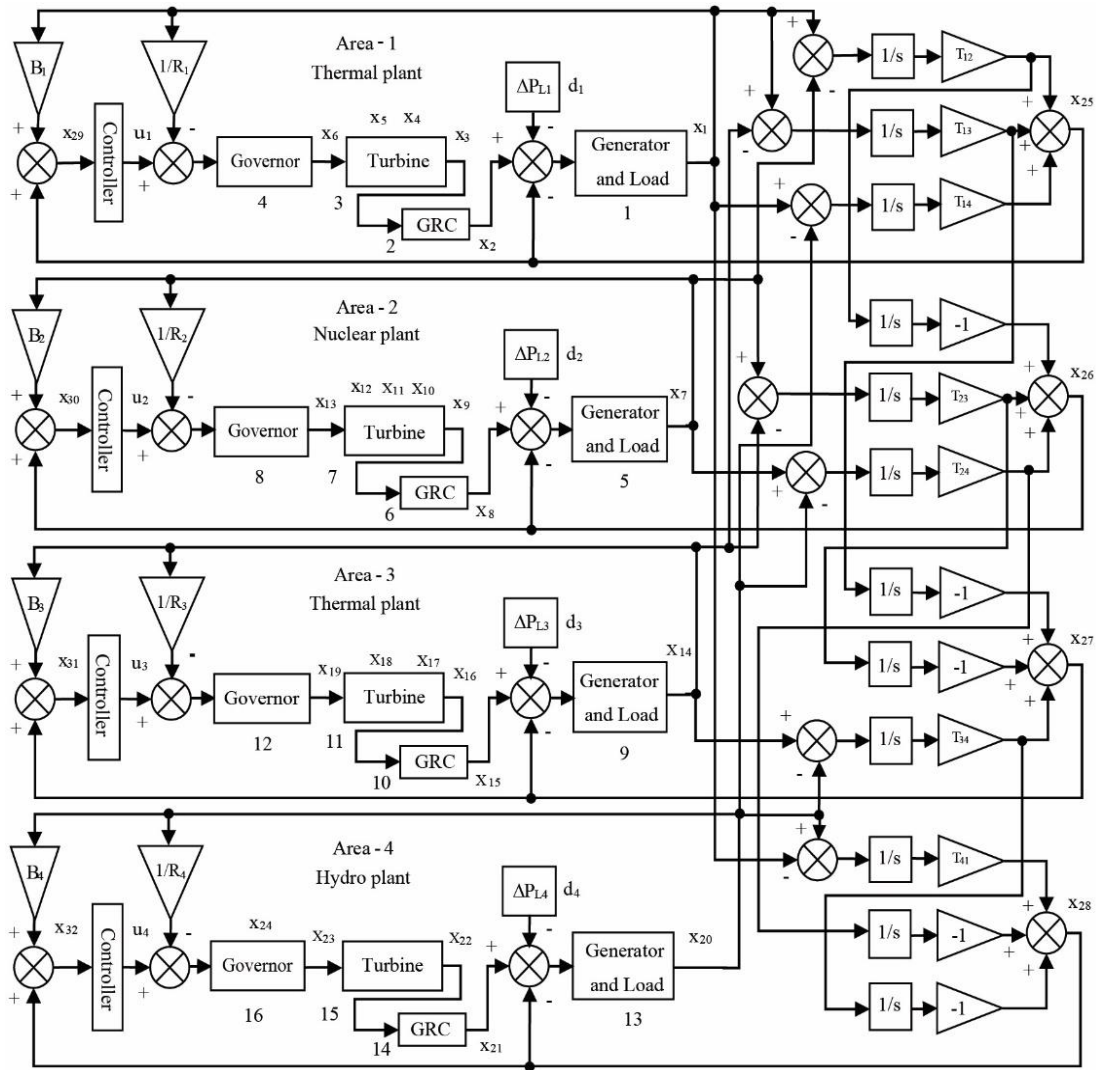
Figure 5. Four area interconnected power system

3. PID AND NARMA-L2 CONTROLLERS
3.1. PID controller
The PID controllers are conventional controllers used when the system requires improvement under steady-state and transient conditions. These controllers design is simple and inexpensive. The Ziegler-Nichols method proposed in [16], [17], is employed to determine the tuned gain values of proportional (K_p), integral (K_i) and derivative (K_d).

3.2. NARMA-L2 controller
The non-linear autoregressive moving average controller is the most effective in the non-linear control systems. It is referred to as NARMA-L2 control when the plant model can be approximated by a particular form [18]–[21]. The dynamic responses of the area frequency and tie-line power flows are obtained using this controller in the power systems [22]. Its main function is to transform non-linear system dynamics into linear dynamics by cancelling the non-linearities.

4. RESEARCH METHOD-OPTIMAL ANN CONTROLLER
In the design of load frequency optimal controller, an artificial neural network (ANN) is to be trained. The flow chart of neural network training process is shown in Figure 6. The training process is divided into three main sections, which are pre-training steps, training the network, and post-training analysis.
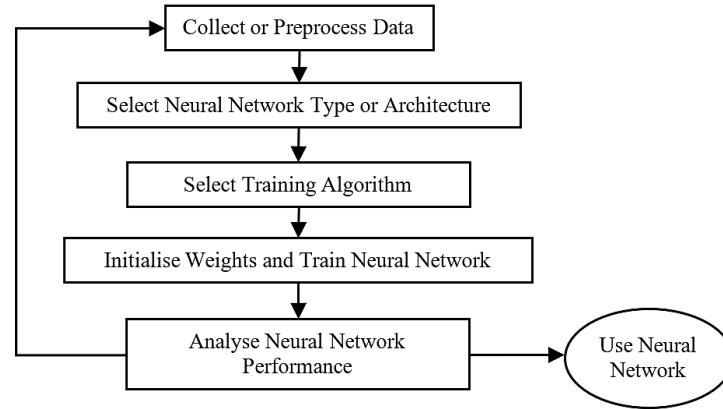
Figure 6. Flow chart of neural network training process

4.1. Data collection and preprocessing

The optimal controller is designed for the power system using state space model [23] with 32 state variables and 4 control output variables. The aim of this controller is to obtain a control law $u(x, t)$ for minimizing the performance index. Formulation of the state space model is achieved by writing differential equations [13], [24] describing each individual block of four area power system in terms of state variables.

These variables are output of various blocks represent the change in mechanical power, electrical power and frequency and are defined as:
- State variables:

$$x_1 = \Delta f_1, x_2 = \Delta P_{m1}, x_3 = \Delta P_{CO1}, x_4 = \Delta P_{RH1}, x_5 = \Delta_{CH1}, x_6 = \Delta P_{V1}, x_7 = \Delta f_2, x_8 = \Delta P_{m2},$$

$$x_9 = \Delta P_{CO2}, x_{10} = \Delta P_{R2}, x_{11} = \Delta P_{R1}, x_{12} = \Delta P_{CH2}, x_{13} = \Delta P_{v2}, x_{14} = \Delta f_3, x_{15} = \Delta P_{m3},$$

$$x_{16} = \Delta P_{CO3}, x_{17} = \Delta P_{RH3}, x_{18} = \Delta P_{CH3}, x_{19} = \Delta P_{V3}, x_{20} = \Delta f_4, x_{21} = \Delta P_{m4}, x_{22} = \Delta P_{HT},$$

$$x_{23} = \Delta P_{HR}, x_{24} = \Delta P_{HG}, x_{25} = \Delta P_{12} + \Delta P_{13} + \Delta P_{14}, x_{26} = \Delta P_{22} + \Delta P_{23} + \Delta P_{24},$$

$$x_{27} = \Delta P_{31} + \Delta P_{32} + \Delta P_{34}, x_{28} = \Delta P_{41} + \Delta P_{42} + \Delta P_{43}, x_{29} = \int ACE_1 \, dt, x_{30} = \int ACE_2 \, dt$$

$$x_{31} = \int ACE_3 \, dt, x_{32} = \int ACE_4 \, dt$$

Control inputs: u_1, u_2, u_3 and u_4, disturbance inputs: $d_1 = \Delta P_{L1}, d_2 = \Delta P_{L2}, d_3 = \Delta P_{L3}$ and $d_4 = \Delta P_{L4}$
- State equations:

$$\text{For block 1: } \dot{x}_1 = -\frac{1}{T_{ps1}} x_1 + \frac{K_{ps1}}{T_{ps1}} x_2 - \frac{K_{ps1}}{T_{ps1}} x_{25} - \frac{K_{ps1}}{T_{ps1}} d_1 \tag{5}$$

$$\text{For block 2: } \dot{x}_2 = x_3 \tag{6}$$

$$\text{For block 3: } \dot{x}_3 = -\frac{1}{T_{tc}} x_3 + \left(\frac{K_{tl}}{T_{tc}} + \frac{K_{ti}}{T_{tc}} - \frac{K_{ti}}{T_{tr}}\right) x_4 + \left(\frac{K_{th}}{T_{tc}} + \frac{K_{ti}}{T_{tr}} - \frac{K_{th}}{T_{tt}}\right) x_5 + \frac{K_{th}}{T_{tt}} x_6$$

$$\dot{x}_4 = -\frac{1}{T_{tr}} x_4 + \frac{1}{T_{tr}} x_5 \quad \text{and} \quad \dot{x}_5 = -\frac{1}{T_{tt}} x_5 + \frac{1}{T_{tt}} x_6 \tag{7}$$

$$\text{For block 4: } \dot{x}_6 = -\frac{1}{R_1 T_{tg}} x_1 - \frac{1}{T_{tg}} x_6 + \frac{1}{T_{tg}} u_1 \tag{8}$$

$$\text{For block 5: } \dot{x}_7 = -\frac{1}{T_{ps2}} x_7 + \frac{K_{ps2}}{T_{ps2}} x_8 - \frac{K_{ps2}}{T_{ps2}} x_{26} - \frac{K_{ps2}}{T_{ps2}} d_2 \tag{9}$$

$$\text{For block 6: } \dot{x}_8 = x_9 \tag{10}$$

For block 7: $\dot{x}_9 = -\frac{1}{T_{nc}}x_9 + \frac{K_{nl}}{T_{nc}}x_{10} + \left(\frac{K_{nh}}{T_{nc}} - \frac{K_{nh}}{T_{nr1}}\right)x_{11} + \left(\frac{K_{nv}}{T_{nc}} - \frac{K_{nv}}{T_{nt}} + \frac{K_{nh}}{T_{nr1}}\right)x_{12} + \frac{K_{nv}}{T_{nt}}x_{13}$

$\dot{x}_{10} = -\frac{1}{T_{nr2}}x_{10} + \frac{1}{T_{nr2}}x_{11}, \dot{x}_{11} = -\frac{1}{T_{nr1}}x_{11} + \frac{1}{T_{nr1}}x_{12}$ and

$$\dot{x}_{12} = -\frac{1}{T_{nt}}x_{12} + \frac{1}{T_{nt}}x_{13} \tag{11}$$

For block 8: $\dot{x}_{13} = -\frac{1}{R_2 T_{ng}}x_7 - \frac{1}{T_{ng}}x_{13} + \frac{1}{T_{ng}}u_2$ (12)

For block 9: $\dot{x}_{14} = -\frac{1}{T_{ps3}}x_{14} + \frac{K_{ps3}}{T_{ps3}}x_{15} - \frac{K_{ps3}}{T_{ps3}}x_{27} - \frac{K_{ps3}}{T_{ps3}}d_3$ (13)

For block 10: $\dot{x}_{15} = x_{16}$ (14)

For block 11: $\dot{x}_{16} = -\frac{1}{T_{tc}}x_{16} + \left(\frac{K_{tl}}{T_{tc}} + \frac{K_{ti}}{T_{tc}} - \frac{K_{ti}}{T_{tr}}\right)x_{17} + \left(\frac{K_{th}}{T_{tc}} + \frac{K_{ti}}{T_{tr}} - \frac{K_{th}}{T_{tt}}\right)x_{18} + \frac{K_{th}}{T_{tt}}x_6$

$$\dot{x}_{17} = -\frac{1}{T_{tr}}x_{17} + \frac{1}{T_{tr}}x_{18} \text{ and } \dot{x}_{18} = -\frac{1}{T_{tt}}x_{18} + \frac{1}{T_{tt}}x_{19} \tag{15}$$

For block 12: $\dot{x}_{19} = -\frac{1}{R_3 T_{tg}}x_{14} - \frac{1}{T_{tg}}x_{19} + \frac{1}{T_{tg}}u_3$ (16)

For block 13: $\dot{x}_{20} = -\frac{1}{T_{ps4}}x_{20} + \frac{K_{ps4}}{T_{ps4}}x_{21} - \frac{K_{ps4}}{T_{ps4}}x_{28} - \frac{K_{ps4}}{T_{ps4}}d_4$ (17)

For block 14: $\dot{x}_{21} = x_{22}$ (18)

For block 15: $\dot{x}_{22} = -\left(\frac{1}{0.5\,R_4\,T_{hg}\left(1+\frac{R_{ht}}{R_h}\right)}\right)x_{20} - \frac{1}{0.5\,T_{hw}}x_{22} +$

$$\left(\frac{1}{0.5\,T_{hw}} + \frac{1}{0.5\,T_{hr}\left(1+\frac{R_{ht}}{R_h}\right)}\right)x_{23} - \left(\frac{1-\frac{T_{hr}}{T_{hg}}}{0.5\,T_{hr}\left(1+\frac{R_{ht}}{R_h}\right)}\right)x_{24} - \left(\frac{1}{0.5\,T_{hg}\left(1+\frac{R_{ht}}{R_h}\right)}\right)u_4 \tag{19}$$

For block 16: $\dot{x}_{23} = -\left(\frac{1}{R_4\,T_{hg}\left(1+\frac{R_{ht}}{R_h}\right)}\right)x_{20} - \left(\frac{1}{T_{hr}\left(1+\frac{R_{ht}}{R_h}\right)}\right)x_{23} +$

$$\left(\frac{1-\frac{T_{hr}}{T_{hg}}}{T_{hr}\left(1+\frac{R_{ht}}{R_h}\right)}\right)x_{24} + \left(\frac{1}{T_{hg}\left(1+\frac{R_{ht}}{R_h}\right)}\right)u_4$$

$$\dot{x}_{24} = -\frac{1}{R_4\,T_{hg}}x_{20} - \frac{1}{T_{hg}}x_{24} + \frac{1}{T_{hg}}u_4 \tag{20}$$

For tie-lines: $\dot{x}_{25} = 2\pi\,T(3x_1 - x_7 - x_{14} - x_{20}), \dot{x}_{26} = 2\pi\,T(3x_7 - x_1 - x_{14} - x_{20})$

$$\dot{x}_{27} = 2\pi\,T(3x_{14} - x_1 - x_7 - x_{20}), \dot{x}_{28} = 2\pi\,T(3x_{20} - x_1 - x_7 - x_{14}) \tag{21}$$

For controller inputs: $\dot{x}_{29} = B_1 x_1 + x_{25}, \dot{x}_{30} = B_2 x_7 + x_{26}, \dot{x}_{31} = B_3 x_{14} + x_{27},$

$$\dot{x}_{32} = B_4 x_{20} + x_{28} \tag{22}$$

Then, the state equation in matrix form:

$$\dot{x} = Ax + Bu + Fd \tag{23}$$

Output equation:

$$y = Cx \tag{24}$$

where the matrix A (32×32) is a coefficient matrix of all the state variables, the matrix B (32x4) is a coefficient matrix of all the control variables, the matrix F (32x4) is a coefficient matrix of all the disturbance variables, the matrix C (1x32) is a coefficient matrix of output variables, $x = [x_1, x_2, \dots, x_{32}]^T$ = state vector, $u = [u_1 \dots u_4]^T$ = control vector and $d = [d_1 \dots d_4]^T$ = disturbance vector.

The optimal control inputs vector, $u = -Kx$ is obtained by a linear combination of all states, where K is the feedback gain matrix. MATLAB code is used to obtain the matrix K by solving of the reduced matrix Riccati equation [6], [9], [20] given by (25):

$$A^T S + SA - SB[R^{-1}B^T S] + Q = 0 \tag{25}$$

where $R^{-1}B^T S = K$ and matrix S is a real, positive definite and symmetric. The matrices Q and R are determined on the basis of three considerations: the excursions of $ACE's, \int ACE\, s\, dt$ and control inputs $u_1 \dots u_4$ about steady values are minimized. These can be recognized as symmetric matrices to minimize performance index in quadratic form, given by (26) and (27).

$$PI = \frac{1}{2} \int_0^\infty (x^T Q\, x + x^T R\, u)\, dt \tag{26}$$

$$PI = \frac{1}{2} \int_0^\infty \begin{bmatrix} (B_1 x_1)^2 + 2B_1 x_1 x_{25} + (x_{25})^2 + (B_2 x_7)^2 + 2B_2 x_7 x_{26} + (x_{26})^2 + (B_3 x_{14})^2 \\ +2B_3 x_{14} x_{27} + (x_{27})^2 + (B_4 x_{20})^2 + 2B_4 x_{20} x_{28} + (x_{28})^2 + (x_{29})^2 + \\ (x_{30})^2 + (x_{31})^2 + (x_{32})^2 + (u_1)^2 + (u_2)^2 + (u_3)^2 + (u_4)^2 \end{bmatrix} dt \tag{27}$$

The discretized system state equations and optimal control inputs vector are used to collect/generate the training data for different values of step load change. Since the time of study and sampling have been chosen as 90 s and 0.005 s respectively, a total of 9000 samples are collected for each variable for a step load change simultaneously in all the four areas. All such variables form one data set, comprises of 40 variables $(x_1, x_2, \dots, x_{32}, d_1 \dots d_4, u_1 \dots u_4)$. Two data sets for each load disturbances have been collected.

4.2. Selecting the neural network architecture

A multilayer feedforward neural network architecture [25] shown in Figure 7 is employed for LFC in a non-linear four-area interconnected power system. The input scalar vector p is represented by a vertical bar with R inputs. There are 36 input nodes (R=36) corresponding to two input parameters which are 32 input nodes, each corresponding to 32 state variables $x_1, x_2, \dots, x_{32}$, and another 4 input nodes for load disturbances or perturbations $(d_1 \dots d_4)$ in the system. The two hidden layers with hyperbolic tangent sigmoid transfer function is used with S neurons to verify the dependency of state variables with the load perturbations and the repeatability of convergence. Hidden layer 1 has $S^1 = 20$ neurons, hidden layer 2 has $S^2 = 10$ neurons, and the output layer has $S^3 = 4$ neurons with linear transfer function are used in the network. The outputs of hidden layers 1 and 2 are the inputs for hidden layer 2 and output layer respectively. The vectors n^1, n^2 and a^3 represent the net inputs, and a^1, a^2 and a^3 represent the outputs of hidden layers 1, 2 and output layer, respectively. For hyperbolic tangent sigmoid transfer function, input/output relations are given by (28).

$$a^1 = \frac{e^{n^1} - e^{-n^1}}{e^{n^1} + e^{-n^1}} \quad and \quad a^2 = \frac{e^{n^2} - e^{-n^2}}{e^{n^2} + e^{-n^2}} \tag{28}$$
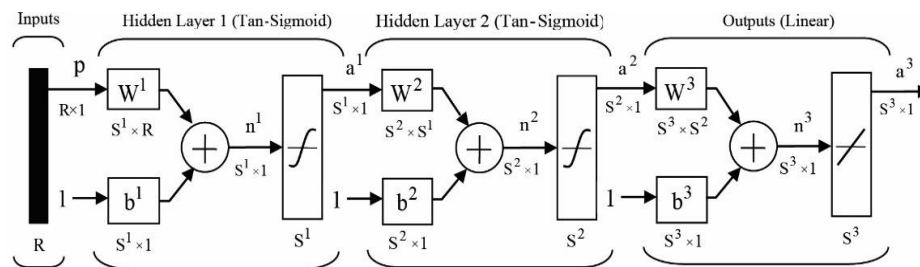

Figure 7. Neural network architecture

For linear transfer function, input/output relation is given by, $a^3 = n^3$ (29)

The outputs of hidden layer 1: $=a^1 = \tan sig(W^1 pxb^1)$ (30)

The outputs of hidden layer 2: $a^2 = \tan sig(W^2 a^1 xb^2)$ (31)

The outputs of output layer: $a^3 = purelin(W^3 a^2 x b^3)$ (32)

where, W^1, W^2 and W^3 represent the weight matrices and b^1, b^2 and b^3 represent bias vectors of hidden layers 1, 2 and output layer respectively. The output of network a^3 is a $(4{\times}1)$ vector represents the target/control signals $(u_1 \dots u_4)$ given to power system corresponding to disturbances $(d_1 \dots d_4)$.

4.3. Neural network training

The network training is based on the data collected from the optimal controller for different perturbations or step load changes. As the inputs are applied to the network, the outputs are compared to the target values, and the supervised learning rule is used. Before network training, initialize the weights and biases using the method of Widrow and Nguyen. In this method, set row i of W^1, $_iW^1$, to have a random direction and a magnitude of $\left| \, _iW^1 \right| = 0.7(S^1)^{1/R}$ and set b_i to a uniform random value between $-\left| \, _iW^1 \right|$ and $\left| \, _iW^1 \right|$. Then, Bayesian regularization backpropagation is used to train the network for 100 epochs because it is very effective algorithm for training multilayer networks and generalized without the need for the validation data set. According to Levenberg-Marquardt optimization, weights and bias values are updated, as it minimizes a combination of squared errors and weights. The performance or mean squared error (MSE) goal is set to a very low value of 1×10^{-10}. Marquardt adjustment parameter and minimum performance gradient are 0.005 and 1×10^{-7} respectively. The training is carried out till the completion of 100 epochs or MSE reaches the desired limit. The network was trained with different number of neurons in the hidden layers. The best MSE value (9.417×10^{-11}) is obtained at epoch 45, as shown in the Figure 8. This algorithm computes the effective number of parameters $(\gamma = 220)$ that are being used by the network. The values of MSE and γ indicate that the network with $S^1 = 20$ and $S^2 = 10$ is satisfactory.
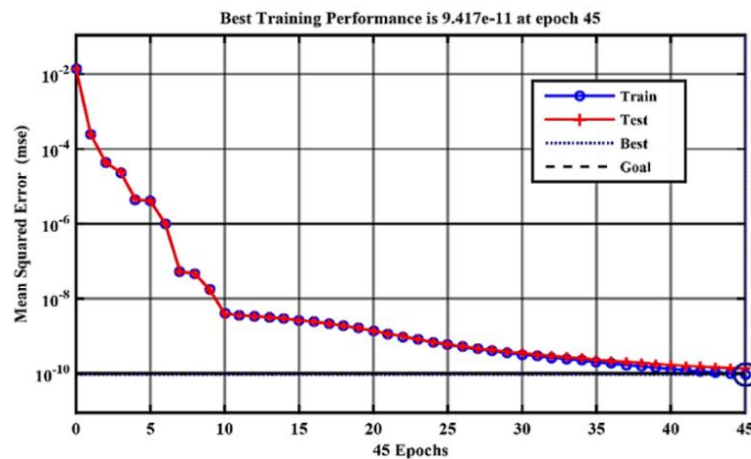

Figure 8. Neural network training error curve

5.   RESULTS AND DISCUSSION

The parameter values of system components are given in Table 1 at base frequency of 50 Hz. The PID controller is tuned by Z-N method and its parameters are shown in Table 2. MATLAB-Simulink is used to perform the simulation of a four-area interconnected power system with three types of controllers. Each of the parameters obtained from the range given in IEEE press power engineering series and EPRI books [26], [27] based on the design of the electrical components for best performance.

Table 1. Power system parameter values

Parameters	P_r	P_L	P_{tie}		f_0	T_{tie}		δ		R	
All Areas	2000 MW	1000 MW	200 MW		50 Hz	0.0866		30°		2.5 Hz/pu MW	
Thermal	T_{tg}	T_{tt}	T_{tr}	T_{tc}	K_{th}	K_{tl}	K_{ti}	D	B	H	K_{ps}	T_{ps}
Plant	0.2s	0.3 s	7 s	0.4s	0.3	0.4	0.3	0.01	0.41	5	100	20s
Nuclear	T_{ng}	T_{nt}	T_{nr1} T_{nr2}	T_{nc}	K_{nv}	K_{nl}	K_{nh}		-	-	-	-
Plant	0.2 s	0.3 s	7 s 7 s	0.4 s	0.22	0.56	0.22	0.01	0.41	5	100	20s
Hydro	T_{hg}	T_{hw}	T_{hr}	R_{th}	R_h	-	-	-	-	-	-	-
Plant	10s	1s	5s	0.2875	0.05	-	-	0.015	0.415	4	66.6667	10.6667s

Table 2. PID controller parameters

Plant	K_{cr}	P_{cr}	K_p	K_i	K_d
Thermal	0.286	12.289	0.1716	0.0279	0.2636
Nuclear	0.1814	19.137	0.1088	0.0114	0.2604
Hydro	0.1119	16.885	0.0671	0.0080	0.1417

MATLAB code is written to obtain optimal controller gain values, to train and test the proposed optimal ANN controller for load frequency control. A step change in load power ΔP_L (steps of 1% up to 5%) in each area is applied. The time domain characteristics-settling time (t_s) and undershoot (M_p), and errors of all four areas are measured and tabulated in Table 3. These specifications are measured using MATLAB function. Figure 9 shows the comparison of frequency deviations in area-1 and area-4 with different controllers under +2% step load change in each area. From Figures 9(a) and 9(b), the change in settling time and maximum undershoot values are measured and tabulated in Table 3. As the load on the system increases suddenly, its frequency decreases at that moment. The maximum undershoot decreases, oscillates, and settle to zero steady state value quickly due to optimal ANN controller action compared to other two controllers. This indicates that the system is stable even with +5% change in load.

It is evident from the Table 3 that the proposed optimal ANN controller gives stable responses with a very minimum steady state error, lesser undershoot, lower settling time and the very smaller values of MSE. Figure 10 shows the frequency deviation with optimal ANN controller under equal and unequal load increase. Figure 10(a) shows for equal load $(\Delta P_{L1} = \Delta P_{L2} = \Delta P_{L3} = \Delta P_{L4} = 4\%)$ in each area. Also, from the Table 3, settling time is 21.8343 s and undershoot is -0.2572 Hz with a MSE value of 1×10^{-10}. These values are smaller compared to that with PID and NARMA-L2 controllers [19], [20] for the same change in load. Figure 10(b) shows the frequency deviation with optimal ANN controller under unequal load increase $(\Delta P_{L1} = 1\%, \Delta P_{L2} = 2\%, \Delta P_{L3} = 3\%, \Delta P_{L4} = 4\%)$ in each area. Under this condition, proposed optimal ANN controller gives good dynamic response with zero steady state error.

The load and frequency deviations in Figure 11 shows the robustness of the proposed optimal ANN controller. Figure 11(a) shows a random load pattern and is more realistic in real power systems. All four areas are encounter this type of load variations [15]. Under this condition, frequency deviation in all areas is shown in Figure 11(b). It reveals that, optimal ANN controller successfully tracks the load pattern and balance generation with load effectively with constant frequency. Only frequency deviation occurs for the equal change in percentage of load in each area, whereas the algebraic sum of change in tie-line power flow is zero.

With optimal ANN controller in the four-area interconnected system, -0.0713 Hz and 23 s are the maximum values of undershoot and settling time for +1% change in load, respectively. For +5% load change, the peak undershoot is -0.3566 Hz and settling time is 22.9970 s. It is seen from the responses with 2% increase in load causes a minimum undershoot of -0.1286 Hz and minimum settling time of 21.864 s. It is observed that, the settling time is constant as the step load increases from 1% to 5%. The magnitude of frequency deviation increases with load, but this increase is very small. On the other hand, as load decreases, the frequency deviation increases with the same settling time. The ITAE values measured with PID and NARMA-L2 controllers [20] are high compared to mean squared error values measured with optimal ANN controller. The time response specification values obtained are smaller compared to their values in literatures [28]–[32].

Table 3. Comparative study of settling time, maximum undershoot and error

| ΔP_L	Controllers	Settling time (s) and error in frequency deviation					Maximum undershoot (Hz) and error in frequency deviation				
		Area-1	Area-2	Area-3	Area-4	ITAE/MSE	Area-1	Area-2	Area-3	Area-4	ITAE/MSE
	PID	37.5065	37.1265	37.5065	36.8291	0.1128	-0.0741	-0.0752	-0.0741	-0.0749	0.1128
+ 1 %	NARMA-L2	15.1145	15.0993	15.1078	26.6548	1e-3	-0.0670	-0.0681	-0.0670	-0.0705	1e-3
	ANN	21.8390	23.0015	21.8396	21.9799	1e-10	-0.0643	-0.0656	-0.0643	-0.0713	1e-10
	PID	31.5815	31.5713	31.5815	31.4318	0.3229	-0.2334	-0.2341	-0.2334	-0.2358	0.3229
+ 2 %	NARMA-L2	18.1999	18.4093	18.2013	18.9832	1e-3	-0.2297	-0.2297	-0.2297	-0.2336	1e-3
	ANN	21.8640	23.0100	21.8640	21.9904	1e-10	-0.1286	-0.1312	-0.1286	-0.1427	1e-10
	PID	25.8792	25.8051	25.8792	25.8254	0.8842	-0.4649	-0.4649	-0.4649	-0.4714	0.8842
+ 3 %	NARMA-L2	23.0941	23.1631	23.0240	22.8366	1e-3	-0.4582	-0.4582	-0.4582	-0.4657	1e-3
	ANN	21.8428	22.9973	21.8439	21.9854	1e-10	-0.1929	-0.1968	-0.1929	-0.2140	1e-10
	PID	48.4521	49.0057	48.4521	47.7849	1.9070	-0.7439	-0.7438	-0.7439	-0.7502	1.9070
+ 4 %	NARMA-L2	31.4917	31.7661	31.4906	32.1603	1e-3	-0.7284	-0.7284	-0.7284	-0.7319	1e-3
	ANN	21.8347	22.9910	21.8343	21.9830	1e-10	-0.2572	-0.2624	-0.2572	-0.2853	1e-10
	PID	53.3577	53.7863	53.3577	52.8282	3.5370	-1.0526	-1.0526	-1.0526	-1.0549	3.5370
+ 5 %	NARMA-L2	33.3008	33.5357	33.4160	33.9808	1e-3	-1.0146	-1.0146	-1.0146	-1.0222	1e-3
	ANN	21.8419	22.9970	21.8414	21.9850	1e-10	-0.3215	-0.3280	-0.3215	-0.3566	1e-10
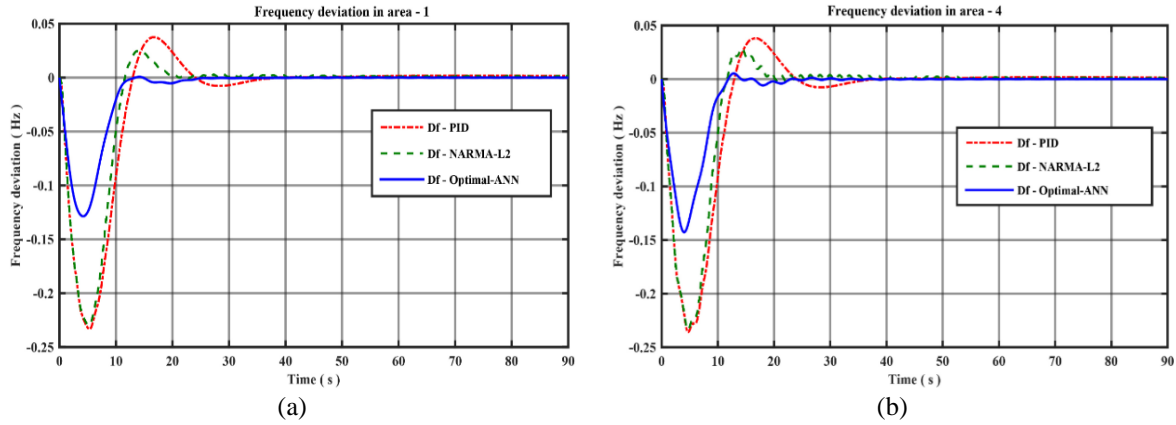
Figure 9. Comparison of frequency deviations in (a) area-1 and (b) area-4 with 2% load increase
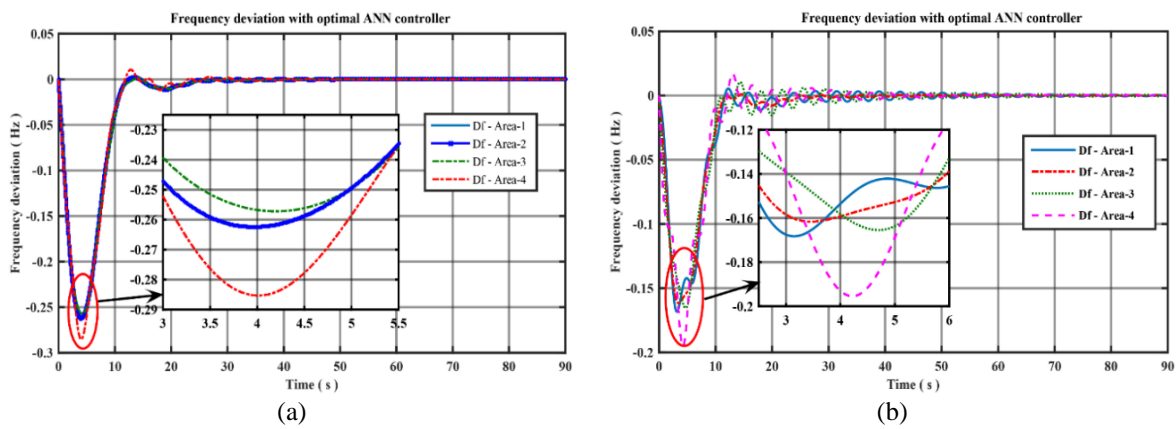

Figure 10. Frequency deviation with optimal ANN controller under (a) +4% load change in each area and (b) unequal load increase in the areas
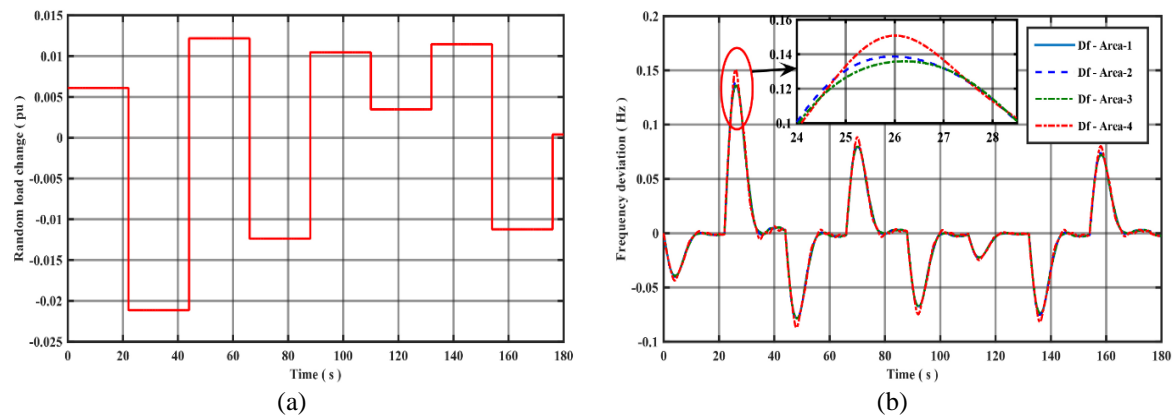

Figure 11. Load and frequency deviations (a) random load pattern and (b) frequency deviation in areas with optimal ANN controller under random step load change

6. CONCLUSION

This study intended to evaluate the performance of optimal ANN controller in a robust LFC problem of a four-area interconnected power system. The system is composed with tandem compound steam turbines and generation rate constraints under different loading conditions. The Z-N rules are used to find the minimum values of ITAE in the design of controllers. The linear quadratic regulator is used to minimize the

performance index and hence the mean squared error. The simulation results for the equal change in percentage of load with proposed optimal ANN controller gives a significant improvement in terms of time response specifications. The settling time, maximum undershoot, and objective function values compared to tuned PID and NARMA-L2 controllers. The conventional controllers give higher values of error due to non-linearity present in the system and loads. The robustness test of proposed optimal ANN controller is carried out with random load pattern. The proposed controller performs satisfactorily under random step load changes and thus desirable dynamic control of the system is achieved.

ACKNOWLEDGEMENTS

REFERENCES

[1] P. Kundur, *Control of active and reactive powers: Active power and frequency control*, 1st ed. New York, USA: McGraw-Hill, 2006.
[2] D. P. Kothari and I. J. Nagrath, *Automatic generation and voltage control*, 4th ed. New Delhi, India: McGraw-Hill, 2013.
[3] H. Bevrani, *Power system control, real power compensation, frequency control, frequency response characteristics and dynamic performance*, 2nd ed. New York, USA: Robust power system frequency control, 2009.
[4] S. Prasad and M. R. Ansari, "Frequency regulation using neural network observer based controller in power system," *Control Engineering Practice*, vol. 102, Sep. 2020, doi: 10.1016/j.conengprac.2020.104571.
[5] D. Qian and G. Fan, "Neural-network-based terminal sliding mode control for frequency stabilization of renewable power systems," *IEEE/CAA Journal of Automatica Sinica*, vol. 5, no. 3, pp. 706–717, May 2018, doi: 10.1109/JAS.2018.7511078.
[6] B. Bhatia, S. Saini, and N. Kumar, "Automatic generation control of multi area power systems using ANN controller," *International Journal of Engineering Science and Technology*, vol. 4, no. 7, pp. 3329–3334, 2012.
[7] N. Chettibi, A. M. Pavan, A. Mellit, A. J. Forsyth, and R. Todd, "Real-time prediction of grid voltage and frequency using artificial neural networks: An experimental validation," *Sustainable Energy, Grids and Networks*, vol. 27, Sep. 2021, doi: 10.1016/j.segan.2021.100502.
[8] K. Alzaareer, A. Q. Al-Shetwi, C. Z. El-bayeh, and M. B. Taha, "Automatic generation control of multi-area interconnected power systems using ANN controller," *Revue d'Intelligence Artificielle*, vol. 34, no. 1, pp. 1–10, Feb. 2020, doi: 10.18280/ria.340101.
[9] S. Prakash and S. K. Sinha, "Simulation based neuro-fuzzy hybrid intelligent PI control approach in four-area load frequency control of interconnected power system," *Applied Soft Computing*, vol. 23, pp. 152–164, Oct. 2014, doi: 10.1016/j.asoc.2014.05.020.
[10] K. Kumari, G. Shankar, S. Kumari, and S. Gupta, "Load frequency control using ANN-PID controller," in *2016 IEEE 1st International Conference on Power Electronics, Intelligent Control and Energy Systems (ICPEICES)*, Jul. 2016, pp. 1–6, doi: 10.1109/ICPEICES.2016.7853516.
[11] S. Prakash and S. K. Sinha, "Automatic load frequency control of six areas' hybrid multi-generation power systems using neuro-fuzzy intelligent controller," *IETE Journal of Research*, vol. 64, no. 4, pp. 471–481, Jul. 2018, doi: 10.1080/03772063.2017.1361869.
[12] A. Mucka, A. Bardhi, and D. Qirollari, "Application of neural networks to load frequency control in power systems with four control areas," *International Journal of Science and Research*, vol. 8, no. 10, pp. 781–787, 2019, doi: 10.21275/ART20201887.
[13] P. S. R. Murthy, *Load frequency control, Control of interconnected systems*, 2nd ed. Hyderabad, India, B. S. Publications, 2008.
[14] F. M. Tuaimah, N. M. Al-Rawi, and W. A. Mahmoud, "Steam turbine governor design based on pole placement technique," *International Journal of Computer Applications*, vol. 92, no. 13, pp. 51–55, Apr. 2014, doi: 10.5120/16073-5306.
[15] E. Sahin, "Design of an optimized fractional high order differential feedback controller for load frequency control of a multi-area multi-source power system with nonlinearity," *IEEE Access*, vol. 8, pp. 12327–12342, 2020, doi: 10.1109/ACCESS.2020.2966261.
[16] K. Ogata, *PID controls, Design of control systems in state space*, 4th ed. New Jersey, USA: Prentice Hall, 2002.
[17] G. S. Thakur and A. Patra, "Load frequency control in single area with traditional Ziegler-Nichols PID tuning controller," *International Journal of Research in Advent Technology*, vol. 2, no. 12, pp. 49–53, 2014.
[18] R. Çelikel, "Speed control of BLDC using NARMA-L2 controller in single lnk manipulator," *Balkan Journal of Electrical and Computer Engineering*, vol. 7, no. 2, Apr. 2019, doi: 10.17694/bajece.510170.
[19] D. K. Sambariya and V. Nath, "Application of NARMA L2 controller for load frequency control of multi-area power system," in *2016 10th International Conference on Intelligent Systems and Control (ISCO)*, 2016, pp. 1–7, doi: 10.1109/ISCO.2016.7726987.
[20] P. Sharma, "NARMA-L2 controller for five-area load frequency control," *Indonesian Journal of Electrical Engineering and Informatics (IJEEI)*, vol. 2, no. 4, pp. 170–179, Dec. 2014, doi: 10.11591/ijeei.v2i4.123.
[21] A. Gundogdu and R. Celikel, "NARMA-L2 controller for stepper motor used in single link manipulator with low-speed-resonance damping," *Engineering Science and Technology, an International Journal*, vol. 24, no. 2, pp. 360–371, Apr. 2021, doi: 10.1016/j.jestch.2020.09.008.
[22] H. Patel, H. Raval, and K. Patil, "Automatic generation control for two area system using artificial neural network based NARMA-L2 controller," *International Journal of Advance Engineering and Research Development*, vol. 3, no. 05, pp. 463–470, May 2016, doi: 10.21090/IJAERD.030571.
[23] N. N. Shah, "The state space modeling of single, two and three ALFC of power system using Integral control and optimal LQR control method," *IOSR Journal of Engineering*, vol. 02, no. 03, pp. 501–510, Mar. 2012, doi: 10.9790/3021-0203501510.
[24] Y. Zhang, X. Liu, and B. Qu, "Distributed model predictive load frequency control of multi-area power system with DFIGs," *IEEE/CAA Journal of Automatica Sinica*, vol. 4, no. 1, pp. 125–135, Jan. 2017, doi: 10.1109/JAS.2017.7510346.
[25] M. T. Hagan, H. B. Demuth, M. H. Beale, and O. De Jesus, *Neuron models and network architectures*, 2nd ed. USA: Martin

Hagan, ch. 2, 2014.

[26]   P. M. Anderson and A. A. Fouad, *"Typical system data" in power system control and stability*, 2nd ed. New Jersey, USA: Wiley-IEEE Press, 2003.

[27]   M. Eremia and M. Shahidehpour, "Active power and frequency control," in *Handbook of electrical power system dynamics-modelling, stability and control*, New Jersey, USA: John Wiley & Sons, Inc, 2013, pp. 291–336.

[28]   K. S. Kumar and A. Prasad, "Load frequency control of hydro-thermal and nuclear interconnected power system using fuzzy and ANN controllers," *International Journal of Science, Engineering and Technology*, vol. 3, no. 3, pp. 582–589, 2015.

[29]   J. Morsali, K. Zare, and M. T. Hagh, "Appropriate generation rate constraint (GRC) modeling method for reheat thermal units to obtain optimal load frequency controller (LFC)," in *2014 5th Conference on Thermal Power Plants (CTPP)*, Jun. 2014, pp. 29–34, doi: 10.1109/CTPP.2014.7040611.

[30]   Y. Wei, I. Jayawardene, and G. K. Venayagamoorthy, "Optimal automatic generation controllers in a multi-area interconnected power system with utility-scale PV plants," *IET Smart Grid*, vol. 2, no. 4, pp. 581–593, 2019, doi: 10.1049/iet-stg.2018.0238.

[31]   N. Patel and B. B. Jain, "Automatic generation control of four area power systems using ANN controllers," *International Journal of Electrical, Electronics and Computer Engineering*, vol. 3, no. 1, pp. 62–68, 2014.

[32]   P. Rani and R. Jaswal, "Automatic load frequency control of multi-area power system using ANN controller and genetic algorithm," *International Journal of Engineering Trends and Technology*, vol. 4, no. 9, pp. 3777–3784, 2013.

BIOGRAPHIES OF AUTHORS

Basavarajappa Sokke Rameshappa 🄸🄳 received his B.E degree in Electrical Engineering from RVCE, Bengaluru University in 1993 and M.E degree in Power Systems from UVCE, Bengaluru University in 1996. He is working as Assistant Professor in Bapuji Institute of Engineering and Technology, Davanagere, Karnataka, India. He has published two papers in an IEEE conference and a journal. He is pursuing his Ph. D at Visvesvaraya Technological University. His research interest includes power systems, load frequency control, control systems and artificial intelligence (AI) techniques. He can be contacted at email: basavarajsr@gmail.com.

Nagaraj Mudakapla Shadaksharappa 🄸🄳 received his B.E degree in Electrical and Electronics in the year 1986 from Government BDT College of Engineering, Davanagere, Karnataka, India. M. Tech degree in Power System from National Institute of Engineering, Mysuru, Karnataka in 1991. Received the Ph. D degree in Electrical Engineering from Visvesvaraya Technological University, Belagavi, Karnataka, India, in 2008. He has published more than 40 papers in National, International Conferences and National Journals. He is currently working as Professor and Head in the Department of Electrical and Electronics Engineering, Bapuji Institute of Engineering and Technology, Davanagere, Karnataka, India. His area of research interest includes electrical distribution systems, and AI applications to power systems. He can be contacted at email: msndvg@gmail.com.